ACADEMIC PRESS

Available online at www.sciencedirect.com
SCIENCE DIRECT®

Journal of Catalysis 215 (2003) 220–233

JOURNAL OF CATALYSIS

www.elsevier.com/locate/jcat

Effect of the chemical composition on the catalytic performance of Mg_yAlO_x catalysts for alcohol elimination reactions

V.K. Díez, C.R. Apesteguía, and J.I. Di Cosimo *

Instituto de Investigaciones en Catálisis y Petroquímica (INCAPE) (UNL-CONICET), Santiago del Estero 2654, (3000) Santa Fe, Argentina

Received 30 August 2002; revised 9 December 2002; accepted 18 December 2002

Abstract

Alcohol C–H bond activation was studied using 2-propanol elimination reactions at 533 K and atmospheric pressure on Mg–Al mixed oxides. Several oxides with Mg/Al ratios of 0.1–9.0 were prepared by thermal decomposition of coprecipitated hydrotalcite-like precursors. Acid and base properties were measured by temperature-programmed desorption of NH_3 and CO_2 coupled with infrared spectra of adsorbed CO_2. The structural composition and homogeneity were investigated by X-ray diffraction and solid-state ^{27}Al NMR (nuclear magnetic resonance). Elimination reactions of 2-propanol on Mg–Al mixed oxides proceeded through reaction pathways occurring on dual acid–base sites (Mg^{2+}–O^{2-} or Al^{3+}–O^{2-}). The chemical nature and acid–base properties of the active sites as well as the catalyst bulk structure and product formation rates for elimination reactions strongly depended on the Mg/Al ratio. In Mg-rich catalysts (Mg/Al $\geqslant 1$), Al^{3+} replaces Mg^{2+} inside the MgO matrix and forms a homogeneous solid without disrupting lattice structure. Elimination reactions occurred on surface Mg^{2+}–O^{2-} pairs via E_{1cB}-like mechanisms that selectively produced the dehydrogenation product (acetone) and to a lesser extent, the dehydration product (propylene). The presence of increasing concentrations of more electronegative Al^{3+} cations decreased the solid average basicity and the catalytic activity. The Al-rich catalysts (Mg/Al < 1) were much more active than the Mg-rich ones, converting 2-propanol mainly to propylene via an E_2 mechanism. The shift in the dehydration reaction mechanism from E_{1cB} (Mg-rich catalysts) to E_2 (Al-rich catalysts) was demonstrated by the existence of two different compensation effect lines, and it was attributed to a change of the active site from Mg^{2+}–O^{2-} to Al^{3+}–O^{2-} and to significant structural modifications. Al-rich samples are structurally heterogeneous oxides that contain a separate quasi-amorphous Al_2O_3-like phase where dehydration takes place at high turnover rates. The surface, structural, and catalytic transition from homogeneous Mg-rich to heterogeneous Al-rich mixed oxides was related to the structural homogeneity of the parent coprecipitated precursor. Whereas a single phase of hydrotalcite-like structure with Mg^{2+} and Al^{3+} cations in close interaction was present in Mg-rich samples, the Al-rich precursors contained Mg^{2+} and Al^{3+} cations in separate hydroxide phases.

Keywords: Alcohol elimination reactions; 2-Propanol; Acid–base catalysis; Hydrotalcites; Alcohol dehydration; Alcohol dehydrogenation

1. Introduction

Calcined hydrotalcite-type anionic clays are widely used in catalysis because of their high surface area, acid–base properties, and structural stability [1]. These materials contain the metal components highly dispersed and in intimate contact, thereby promoting complex bifunctional reactions, which require the catalyst functions to exist in mutual contact within atomic dimensions.

In particular, hydrotalcite-derived Mg–Al mixed oxides present acid or base properties depending on the chemical composition and preparation procedures [2,3]. Promising applications of these materials for synthesis of both fine chemicals and commodities have been recently reported [4]. Mg–Al mixed oxides catalyze a variety of reactions requiring anionic intermediates, such as aldol condensation reactions of aldehydes and ketones in either the gas or the liquid phase [5–7], alkylations [8,9], Knoevenagel condensations [10], Michael additions [11], cyanoethylation of alcohols [12], and double-bond isomerization of alkenes [13], among other useful applications involving a C–H bond cleavage step. Other novel applications include alkoxylation of alcohols [14,15], and oxidation of mercaptan [16].

Recently, we investigated the catalytic properties of hydrotalcite-derived Mg–Al mixed oxides to promote sev-

* Corresponding author.
E-mail address: dicosimo@fiqus.unl.edu.ar (J.I. Di Cosimo).

0021-9517/03/$ – see front matter
doi:10.1016/S0021-9517(03)00010-1

eral reactions involving primary and secondary alcohols, such as the self-condensation of ethanol [17], the cross-coupling of methanol and 1-propanol [18], and the one-step synthesis of methyl isobutyl ketone from 2-propanol [19]. We found that Mg–Al mixed oxides efficiently catalyze alcohol coupling reactions by promoting C–C bond formation, a reaction step that takes place after C–H bond activation. We also found [17,18] that the catalytic activity and selectivity depended not only on the density and strength of the surface base sites but also on the structural changes produced in the mixed oxides upon increase of the Al content.

As a continuation of the work with primary alcohols, we have now addressed our investigations toward the activation of C–H bonds of secondary alcohols using 2-propanol elimination reactions. Elimination reactions are involved in the reaction mechanism of important industrial processes. For example, hydrogen and water abstractions occur by C–H bond rupture and they are key steps in the mechanism of coupling reactions (aldol-like condensations or alkylations) and olefin isomerization or aromatization.

2-Propanol can be converted via elimination reactions such as dehydrogenation and dehydration which proceed through different mechanisms depending on the catalyst acid–base properties. It is generally accepted that strong Brønsted solid acids dehydrate 2-propanol to propylene by an E_1 mechanism, whereas on amphoteric oxides 2-propanol is transformed to ether and, in a concerted E_2 mechanism occurring on surface dual acid–base sites of balanced strength, to olefin [20]. However, dehydration can also take place on basic catalysts containing acid–base pairs of imbalanced strength through an E_{1cB} mechanism [20]. On the other hand, only on strongly basic catalysts 2-propanol is preferentially dehydrogenated to acetone [21–23].

In this paper, we study 2-propanol elimination reactions on Mg–Al mixed oxides. Our goal was to elucidate 2-propanol elimination reaction pathways and to ascertain the nature of the surface sites and structures that promote these reactions on Mg–Al mixed oxides of different chemical compositions.

We examine by X-ray diffraction and solid state ^{27}Al NMR the structural composition of Mg–Al catalysts prepared from hydrotalcite-like precursors. The nature, density, and strength distribution of surface acid and base sites are probed by temperature-programmed desorption of NH_3 and CO_2 coupled with infrared spectra of adsorbed CO_2.

We discuss the effect of chemical composition on the surface and structural properties and on the catalytic performance of Mg–Al mixed oxides. To our knowledge, there is no report in the literature analyzing these effects in a wide compositional range covering Mg/Al molar ratios from 0.1 to 9.0. The different catalytic behavior observed between Mg-rich and Al-rich Mg–Al mixed oxides is interpreted in terms of the type of structure and structural homogeneity of both the parent precursor and the oxide itself.

2. Experimental

2.1. Catalyst preparation

A set of Mg–Al hydrotalcite-like precursors with different Mg/Al atomic ratio (y) was prepared by the coprecipitation method at a constant pH of 10 as previously described [17]. An aqueous solution of the metal nitrates with a total [Mg + Al] cation concentration of 1.5 M was contacted with a basic solution of K_2CO_3 and KOH by dropwise addition of both solutions into a stirred beaker containing 350 cm^3 of distilled deionized water held at 333 K. The precipitates formed were aged in their mother liquor for 2 h at 333 K and then filtered, washed with boiling distilled water until K^+ was no longer detected in the filtrate, and dried at 348 K overnight. These precursors were decomposed in N_2 at 673 K overnight in order to obtain the corresponding Mg–Al mixed oxides (Mg_yAlO_x samples). Pure alumina and MgO were prepared following the same procedure.

2.2. Catalyst characterization

The solid structure of the Mg–Al hydroxycarbonate precursors and of the Mg–Al mixed oxides were determined by powder X-ray diffraction methods (XRD) using a Shimadzu XD-D1 diffractometer and Ni-filtered Cu-K_α radiation.

MAS (magic-angle spinning) ^{27}Al NMR (nuclear magnetic resonance) spectra were obtained on a Bruker AV-400 spectrometer at ambient temperature and at 104.2 MHz using a Bruker MAS probe with zirconia rotors (2.5 mm diameter) and a sample spinning rate of 20 kHz. The length of de rf pulses was 1.0 μs. A total amount of 1000 fids was accumulated and a time interval of 1.0 s between successive fids was selected to avoid saturation effects. All measurements were carried out at room temperature with kaolinite as a standard reference. Samples were pretreated in vacuum for 1 h at 673 K and then loaded into the rotor in a glove box.

CO_2 adsorption site densities and binding energies were obtained from temperature-programmed desorption (TPD) of CO_2 preadsorbed at room temperature. Samples (50–150 mg) were treated in N_2 at 673 K for 1 h and exposed to a 3.09% CO_2/N_2 stream until saturation coverages were reached. Weakly adsorbed CO_2 was removed by flushing with N_2 at room temperature for about 1 h. The temperature was then increased at 10 K/min from 298 to 673 K. The evolved CO_2 was converted to methane by means of a methanation catalyst (Ni/Kieselghur) operating at 673 K and monitored using a flame ionization detector.

The structure of CO_2 chemisorbed on Mg_yAlO_x samples was determined by infrared spectroscopy (IR). Data were obtained using a Shimadzu FTIR-8101M spectrophotometer after admission of 5.3 kPa of CO_2, adsorption at room temperature, and sequential evacuation at 298, 373, 473, and 573 K. Spectra were taken at room temperature. An inverted

Table 1
Chemical composition, BET surface areas, and XRD characterization of MgO, Al_2O_3, and Mg_yAlO_x mixed oxide samples

Sample	r[a]	Chemical analysis by AAS				S_g	Structural analysis by XRD			
	(nominal)	r[a]	Mg	Al	K	(m^2/g)	Coprecipitated precursors		Mg_yAlO_x	
			(wt%)	(wt%)	(wt%)		Phases detected	a (Å)	Phases detected	a (Å)
MgO	0.00	0.00	–	–	–	185	Brucite	3.148	MgO periclase	4.220
Mg_9AlO_x	0.10	0.11	43.7	5.8	0.008	114	Hydrotalcite + brucite	3.132	MgO periclase	4.208
Mg_5AlO_x	0.17	0.18	39.7	9.7	0.02	184	Hydrotalcite	3.068	MgO periclase	4.211
Mg_3AlO_x	0.25	0.24	34.4	12.1	0.02	238	Hydrotalcite	3.052	MgO periclase	4.216
Mg_1AlO_x	0.50	0.47	22.2	21.5	0.071	231	Hydrotalcite	3.019	MgO periclase	4.209
$Mg_{0.5}AlO_x$	0.67	0.66	13.0	27.6	0.014	296	Hydrotalcite + brucite + gibbsite	3.020	$MgAl_2O_4 + MgO + \gamma$-Al_2O_3 (qa)	–
$Mg_{0.33}AlO_x$	0.75	0.76	8.7	30.0	0.02	301	Brucite + gibbsite + hydrotalcite (t)	–	γ-Al_2O_3 (qa)	–
$Mg_{0.2}AlO_x$	0.83	0.86	5.2	35.0	0.015	243	Brucite + gibbsite	–	γ-Al_2O_3 (qa)	–
$Mg_{0.11}AlO_x$	0.90	0.91	3.4	37.4	0.025	240	Brucite (t) + gibbsite	–	γ-Al_2O_3 (qa)	–
Al_2O_3	1.00	1.00	–	–	–	388	Gibbsite	–	γ-Al_2O_3 (qa)	–

[a] $r = Al/(Al + Mg)$ molar ratio; (t), traces; (qa), quasi-amorphous.

T-shaped Pyrex cell containing the sample pellet was used. The two ends of the short arm of the T were fitted with CaF_2 windows. The absorbance scales were normalized to 50-mg pellets.

Acid site densities were determined by using TPD of NH_3. Samples (150 mg) were treated in He (~ 100 cm^3/min) at 673 K for 0.5 h and exposed to a 1.01% NH_3/He stream at room temperature until surface saturation. Weakly adsorbed NH_3 was removed by flowing He at 60 cm^3/min for 0.5 h. Temperature was then increased to 673 K at 10 K/min, and the NH_3 concentration in the effluent was measured by mass spectrometry (MS).

Bulk elemental analysis of Mg, Al, and K was carried out by atomic absorption spectroscopy (AAS). Total surface areas (S_g) were measured by N_2 physisorption at 77 K using a Quantachrome Nova-1000 sorptometer and BET analysis methods.

2.3. Catalytic testing

2-Propanol (Merck ACS, 99.5% purity) elimination reactions were carried out at 533 K and 100 kPa in a differential fixed-bed tubular reactor. Samples were sieved to retain particles with 0.35–0.42 mm diameters for catalytic measurements and treated in N_2 at 673 K for 1 h before reaction in order to remove adsorbed H_2O and CO_2. The reactant was introduced as 1/15 2-propanol/N_2 mixture. Typical space velocities (WHSV) were in the range of 2–200 h^{-1} in order to keep 2-propanol conversions below 5%. Reaction products were analyzed by on-line gas chromatography in a Varian Star 3400 CX chromatograph equipped with a flame ionization detector and a Porapak R column. Data were collected every 20 min for 10 h. Reaction products were acetone (C_3one), propylene (C_3=) and diisopropyl ether (DIPE).

3. Results

3.1. Characterization of Mg–Al precursors and M_yAlO_x samples

Precipitated Mg–Al precursors of different aluminum molar composition, defined as $r = Al/(Al + Mg)$, were analyzed by XRD and the crystalline phases detected are shown in Table 1. Precursors are hydroxycarbonates with a single crystalline phase of hydrotalcite structure for values of r in the range of $0.67 > r > 0.1$. The hydrotalcite structure, $[Mg_{1-r}Al_r(OH)_2]^{r+}(CO_3{}^{2-})_{r/2} \cdot mH_2O$ (ASTM 14-191), consists of layered double hydroxides with brucite-like layers in which Mg and Al cations are in close interaction and share octahedral positions. The interlayer spacing is occupied by charge-compensating $CO_3{}^{2-}$ anions and by weakly bonded water molecules. Sharp X-ray diffraction lines were detected in the precursor with $r = 0.25$, which has the composition of the stoichiometric hydrotalcite, $Mg_6Al_2(OH)_{16}CO_3 \cdot 4H_2O$. All the other hydrotalcite-containing precursors showed broader XRD lines, corresponding to smaller crystallites or less ordered structures.

Outside of the $0.67 > r > 0.1$ range, additional crystalline hydroxide phases of Mg [$Mg(OH)_2$, brucite, ASTM 7-239] or Al [$Al(OH)_3$, gibbsite, ASTM 7-324] were observed. No hydrotalcite phase was detected in precursors with $r \geqslant 0.83$.

The unit cell constants (a and c) for hydrotalcite structures with hexagonal 3R symmetry were calculated from X-ray diffraction patterns on all the hydrotalcite-containing precursors and the values of a are shown in Table 1. The a values decreased linearly following a Vegard's law dependence as the Al content increases from the initial value of the Al-free brucite phase (3.148 Å) to 3.019 Å for the precursor with $r = 0.5$. No further contraction of the unit cell (3.020 Å) was found when the Al content was augmented up to a value of $r = 0.67$.

The chemical composition, BET surface area, and crystalline phases for Mg_yAlO_x mixed oxides, MgO, and Al_2O_3

are also shown in Table 1. Elemental analysis of mixed oxides revealed that the measured atomic ratios r were very similar to the nominal values, suggesting complete precipitation of Mg and Al salts during synthesis. The potassium content in all the mixed oxides was below 0.1 wt%, which confirms that K^+ ions were effectively removed by washing of the precipitated precursors.

The diffraction patterns of Mg-rich mixed oxides ($r \leqslant 0.5$) showed the presence of a single crystalline MgO periclase phase (ASTM 4-0829) with no residual traces of hydrotalcite or hydroxide phases, thereby indicating that heating at 673 K completely decomposes the precursor samples. The crystallinity of MgO phase decreased with increasing r from 0 to 0.5. No crystalline AlO_x phases were observed on Mg-rich mixed oxides ($r \leqslant 0.5$), which suggests that the Al^{3+} cations remained closely associated within the MgO structure after thermal decomposition of precipitated precursors. However, no contraction of the MgO lattice was determined in the calculations of the lattice parameter of the cubic periclase structure (Table 1) probably due to the poor crystallinity of the MgO phase.

In Mg_yAlO_x samples of high Al content ($r > 0.5$), a quasi-amorphous Al_2O_3 phase (ASTM 10-425) was detected, suggesting that Al^{3+} cations lost the intimate contact with the MgO matrix. In sample $Mg_{0.5}AlO_x$ ($r = 0.67$), an additional $MgAl_2O_4$ spinel phase (ASTM 21-1152) was also found showing the transition between Mg-rich and Al-rich catalysts.

Analysis of the MAS ^{27}Al NMR spectra of Mg_yAlO_x mixed oxides and Al_2O_3 showed two resonance lines in the regions around 64–70 and 7–15 ppm, which correspond to Al^{3+} cations tetrahedrally (Al_{Td}) and octahedrally (Al_{Oh}) coordinated to oxygen, respectively [24,25]. Chemical shifts as a function of the chemical composition are presented in Fig. 1. The experimental points for Al_{Oh} may be fitted with a broken line in which Mg-rich ($r \leqslant 0.5$) and Al-rich ($r > 0.5$) samples are clearly grouped. In contrast, a linear dependence is observed between Al_{Td} and r. Both Al_{Oh} and Al_{Td} chemical shifts diminish with increasing r because Mg^{2+} is gradually replaced by more electronegative Al^{3+} as the nearest neighbor cation bonded to the Al–O polyhedra [24]. Thus, the smallest chemical shifts (64.1 and 6.9 ppm for Al_{Td} and Al_{Oh} bands, respectively) were measured on pure alumina, which contains the Al–O polyhedra surrounded exclusively by Al^{3+} cations as nearest neighbors.

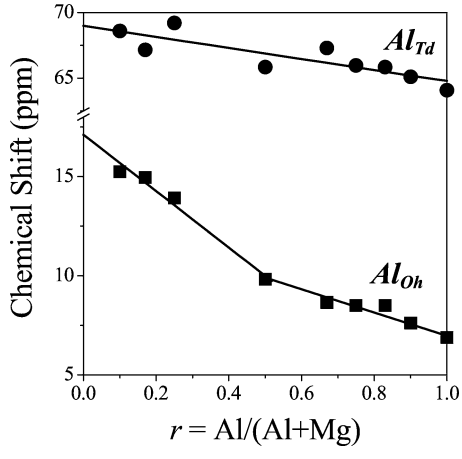

Fig. 1. ^{27}Al NMR analysis of Mg_yAlO_x and Al_2O_3 samples. Chemical shifts for octahedrally and tetrahedrally coordinated aluminum as a function of the chemical composition.

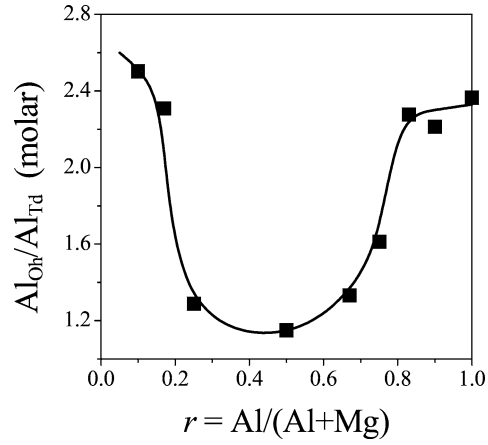

Fig. 2. ^{27}Al NMR analysis of Mg_yAlO_x and Al_2O_3 samples. Effect of the chemical composition on Al_{Oh}/Al_{Td} molar ratio.

The MAS ^{27}Al NMR spectra were deconvoluted in two contributions and the integrated peak intensities were used to determine the Al_{Oh}/Al_{Td} molar ratio for each Mg_yAlO_x mixed oxide (Fig. 2). All the samples contained the Al^{3+} cations preferentially located in octahedral positions ($2.50 \geqslant Al_{Oh}/Al_{Td} \geqslant 1.15$), but Mg-rich and Al-rich samples showed the highest Al_{Oh}/Al_{Td} values giving rise to an inverted volcano curve when Al_{Oh}/Al_{Td} is represented as a function of r (Fig. 2). About 30% of the Al^{3+} cations of alumina were in tetrahedral coordination ($Al_{Oh}/Al_{Td} = 2.36$), in agreement with results of McKenzie et al. [25]. Alumina can be regarded as a defect spinel phase in which the Al_{Oh}/Al_{Td} ratio is usually in the range of 1.67–3.00 and the cationic vacancies are distributed in octahedral and tetrahedral sites [26]. On the $Mg_{0.5}AlO_x$ ($r = 0.67$) sample, which has the bulk stoichiometric composition of the spinel phase, 43% the Al^{3+} cations were in tetrahedral positions ($Al_{Oh}/Al_{Td} = 1.33$). The unit cell of the natural $MgAl_2O_4$ has a normal spinel structure with 32 oxygens and 24 cations ($8Mg^{2+}$ tetrahedrally coordinated and $16Al^{3+}$ octahedrally coordinated) [27,28]. However, synthetic Mg–Al spinels prepared by thermal decomposition of hydrated precursors at low temperatures usually present partially inverse spinel structures which contain 40–50% of the Al^{3+} cations and 10–20% of the Mg^{2+} cations in tetrahedral positions [24,29].

Finally, the Al_{Oh} and Al_{Td} contents (wt%) were calculated by combining the Al_{Oh}/Al_{Td} ratio and the bulk chemical composition reported in Table 1. The Al_{Oh} content increased monotonically with r reaching 37.2 wt% for pure

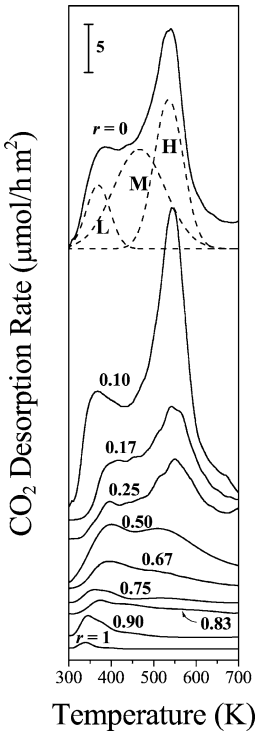

Fig. 3. TPD profiles of CO_2 on MgO, Al_2O_3, and Mg_yAlO_x samples. CO_2 adsorption at 298 K, 10 K/min heating rate, $r = Al/(Al + Mg)$.

alumina while the amount of Al_{Td} gradually increased up to about 11 wt% for sample Mg_1AlO_x ($r = 0.50$) but then remained approximately constant for samples containing higher Al content ($r > 0.50$).

The nature of chemisorbed CO_2 species and a measure of the base site density were obtained by combining TPD and infrared measurements of CO_2 preadsorbed at room temperature. The CO_2 desorption rate as a function of sample temperature is presented in Fig. 3 for MgO, Al_2O_3, and Mg_yAlO_x samples. The total amount of desorbed CO_2 was measured by integration of TPD curves. The resulting values are reported in Table 2. In general, the base site density decreased with increasing catalyst Al content.

The complex TPD profiles suggest that the surfaces of MgO and mixed oxide samples are nonuniform and contain several types of adsorbed CO_2. To investigate the probable formation of more than one CO_2 adsorbed species, and consequently the presence of surface base sites (oxygen anions) of different chemical nature, IR spectra of CO_2 adsorbed at room temperature were taken after sequential evacuation at increasing temperatures. Fig. 4 shows the IR spectra obtained on Mg_9AlO_x and $Mg_{0.2}AlO_x$ samples, which typically represent similar spectra obtained on Mg-rich and Al-rich samples, respectively. The spectra of pure MgO and Al_2O_3 were included as reference. Broad infrared bands were observed on MgO and Mg_yAlO_x samples in the 1700–1300 cm^{-1} region following the CO_2 adsorption. We identified three adsorption species (schematically represented in Fig. 4), which apparently reflect three surface base sites of different chemical nature and binding energies: unidentate and bidentate carbonate, and bicarbonate [17,30]. Unidentate carbonate formation requires low-coordination oxygen anions (strong base sites), such as those of pure MgO. On Mg-rich samples, bidentate carbonate forms on acid–base pairs such as Mg^{2+}–O^{2-} (intermediate strength base site) whereas on Al-rich samples the bidentate species is more likely formed on Al^{3+}–O^{2-} pairs. Bicarbonate forms on MgO, Al_2O_3, and all the Mg_yAlO_x samples; it involves surface hydroxyl groups that can be considered as weak base sites on Mg-rich samples [31] or as weak acid sites on Al-rich samples. Bicarbonate was clearly the predominant species formed on Al_2O_3 upon CO_2 adsorption at room temperature and it was removed completely from the alumina surface after evacuation at 373 K. Then, upon desorption at temperatures higher than 373 K, bidentate carbonates formed on Al^{3+}–O^{2-} pairs are the only species remaining on pure alumina.

Based on the above IR characterization, the TPD profiles of Fig. 3 were deconvoluted in three desorption bands: a low-

Table 2
Characterization of acid–base surface properties of MgO, Al_2O_3, and Mg_yAlO_x samples

Sample	Density of base sites[a] (μmol/m^2)				Density of acid sites[b] (μmol/m^2)		
	L[c,d]	M[c,d]	H[c,d]	Total evolved CO_2	L[c,d]	H[c,d]	Total evolved NH_3
MgO	0.79 (13.7)	2.68 (46.7)	2.27 (39.6)	5.74	0.08 (66.0)	0.04 (34.0)	0.12
Mg_9AlO_x	0.81 (11.0)	3.72 (50.2)	2.87 (38.8)	7.40	0.14 (86.0)	0.02 (14.0)	0.16
Mg_5AlO_x	0.33 (9.0)	1.95 (54.6)	1.30 (36.4)	3.58	0.10 (80.3)	0.03 (19.7)	0.13
Mg_3AlO_x	0.29 (11.2)	1.40 (54.2)	0.90 (34.6)	2.59	0.09 (89.5)	0.01 (10.5)	0.10
Mg_1AlO_x	0.37 (14.7)	1.16 (47.0)	0.95 (38.3)	2.48	0.16 (86.0)	0.02 (14.0)	0.18
$Mg_{0.5}AlO_x$	0.25 (27.3)	0.38 (41.8)	0.28 (30.9)	0.91	0.19 (68.8)	0.09 (31.2)	0.28
$Mg_{0.33}AlO_x$	0.14 (34.4)	0.14 (36.1)	0.12 (29.5)	0.40	0.25 (68.3)	0.12 (31.7)	0.37
$Mg_{0.2}AlO_x$	0.26 (40.5)	0.23 (36.6)	0.15 (22.9)	0.64	0.42 (72.5)	0.16 (27.5)	0.58
$Mg_{0.11}AlO_x$	0.16 (61.0)	0.10 (39.0)	0.00 (0.0)	0.26	0.34 (58.9)	0.23 (41.1)	0.57
Al_2O_3	0.04 (66.2)	0.02 (33.8)	0.00 (0.0)	0.06	0.36 (45.0)	0.45 (55.0)	0.81

[a] TPD of adsorbed CO_2.
[b] TPD of adsorbed NH_3.
[c] L, low-temperature peak; M, middle-temperature peak; H, high-temperature peak.
[d] The percentage of contribution of each peak is in parentheses.

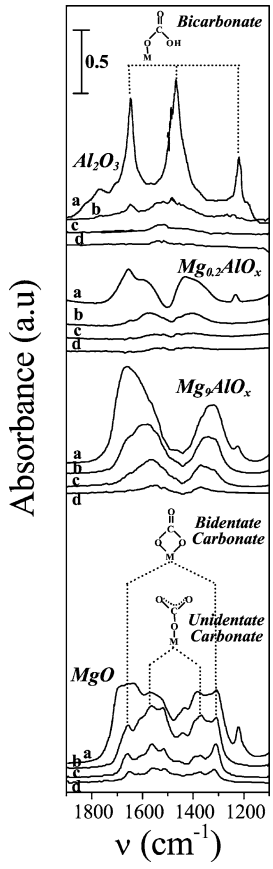

Fig. 4. Infrared spectra of CO_2 preadsorbed on MgO, Mg_9AlO_x, $Mg_{0.2}AlO_x$, and Al_2O_3 samples upon desorption at increasing temperatures: (a) 298 K, (b) 373 K, (c) 473 K, (d) 573 K. CO_2 adsorption at 298 K.

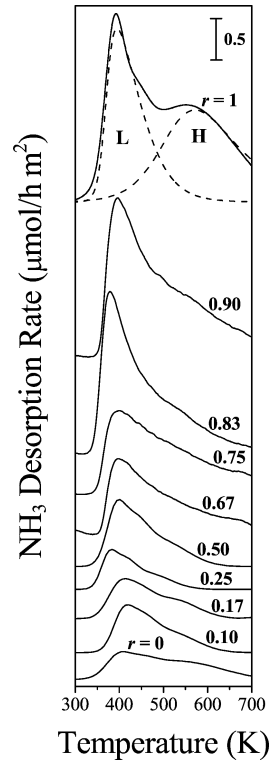

Fig. 5. TPD profiles of NH_3 on MgO, Al_2O_3, and Mg_yAlO_x samples. NH_3 adsorption at 298 K, 10 K/min heating rate, $r = Al/(Al + Mg)$.

temperature (L-peak) at 370–400 K, assigned to bicarbonates formed on Brønsted OH groups; a middle-temperature (M-peak) at 460 K attributed to bidentate carbonates desorbed from metal–oxygen pairs; and a high-temperature peak (H-peak) at 550 K resulting from unidentate carbonates released from low coordination oxygen anions. Results are shown in Table 2. The M-peak and H-peak are dominant on MgO and Mg_yAlO_x samples with $r \leqslant 0.5$. In Al-rich samples ($r > 0.5$), the relative contribution of the high- and middle-temperature peaks decreases with increasing Al content at the expense of the low-temperature peak, thereby decreasing the average basicity. Pure Al_2O_3 and $Mg_{0.11}AlO_x$ samples showed no contribution of the high-temperature peak in their TPD profiles.

Acid surface properties of Mg_yAlO_x, MgO, and Al_2O_3 samples were investigated by TPD of NH_3 preadsorbed at room temperature as presented in Fig. 5. Acid site densities determined by integration of the TPD profiles are presented in Table 2. The total NH_3 evolved from the samples is similarly low on MgO and Mg-rich samples ($r \leqslant 0.5$), but increases almost linearly with increasing Al content on Mg_yAlO_x samples with $r > 0.5$. The NH_3 TPD on Al_2O_3 shows that NH_3 desorbs in two overlapping signals, a low-temperature peak at about 400 K and a high-temperature peak at 575 K. Since the NH_3 adsorption was performed at room temperature, the L-peak may be attributed to reversible H-bonded adsorption on Brønsted sites whereas the H-peak was assigned to the irreversible coordinated adsorption on Lewis acid sites of alumina [3,32]. Similar peak deconvolutions were carried out for NH_3 TPD on Mg_yAlO_x and MgO samples. In all the samples, surface hydroxyl groups can account for the Brønsted acidity. Shen et al. [24], based on IR and calorimetric measurements of the NH_3 adsorption on Al_2O_3 and Mg–Al mixed oxides, attributed the Lewis acidity on Mg-rich Mg_yAlO_x samples to surface defects with accessible Al^{3+} cations in Al^{3+}–O^{2-}–Mg^{2+} species whereas on alumina, the Lewis acidity was more likely assigned to Al^{3+} cations in the abundant surface Al^{3+}–O^{2-} pairs. The H-peak of MgO, on the other hand, may result not only from the irreversible coordinated NH_3 adsorption on Mg^{2+} cations but also from the heterolytic dissociative adsorption leading to NH_2^-–H^+ species on Mg^{2+}–O^{2-} pairs [3,33].

The density of Brønsted acid sites on Mg_yAlO_x samples was higher than that of Lewis sites, but the relative contribution of Lewis acid sites to the sample acidity increased with increasing Al content (Table 2). On alumina, the Lewis acidity was predominant.

3.2. Conversion of 2-propanol on Mg_yAlO_x mixed oxides

The catalytic conversion of 2-propanol via elimination reactions was studied at 533 K and atmospheric pressure on MgO, Al_2O_3, and Mg_yAlO_x mixed oxides. At low conversions, 2-propanol is converted on Mg_yAlO_x mixed oxides

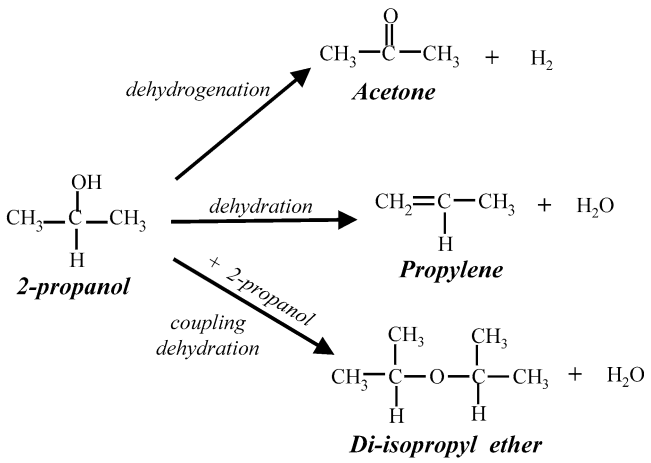

Scheme 1. Reaction network of 2-propanol conversion on Mg_yAlO_x catalysts.

via three parallel reactions: dehydrogenation, dehydration, and coupling-dehydration as shown in Scheme 1 [34,35]. The main products of 2-propanol elimination reactions were acetone (C_3H_6O), propylene (C_3H_6), and to a lesser extent, diisopropyl ether ($C_3H_7OC_3H_7$).

Fig. 6 illustrates the typical time-on-stream behavior of Mg_yAlO_x mixed oxides during 2-propanol elimination reactions. Sample Mg_3AlO_x (Fig. 6A) formed acetone (C_3one) and propylene (C_3=) as the main products and minor amounts of DIPE. Sample $Mg_{0.2}AlO_x$ yielded primarily C_3= (Fig. 6B).

All the Mg_yAlO_x samples deactivated during the catalytic experiments and lost about 50% of activity after the 10 h run. Thus, initial 2-propanol conversion rate (R^0) and product formation rates (R_i^0) were calculated by extrapolating the reaction rates vs time curves to zero.

The 2-propanol initial conversion rate on MgO, Al_2O_3, and Mg_yAlO_x mixed oxides as a function of composition is presented in Fig. 7. The R^0 values were strongly dependent on the Al content and the catalyst set may be divided in two groups showing different catalytic behavior. As indicated in Fig. 7 by the dashed line, there is a catalytic activity break at a r value slightly higher than 0.5. Sample Mg_1AlO_x ($r = 0.5$, $R^0 = 2.8$ μmol/h m^2) was, in fact, about two orders of magnitude less active for converting 2-propanol than sample $Mg_{0.5}AlO_x$ ($r = 0.67$, $R^0 = 194.1$ μmol/h m^2). MgO and Mg-rich Mg_yAlO_x oxides ($r \leqslant 0.5$) constitute the first group of samples and showed poor activity to decompose 2-propanol. MgO was the most active sample in this group since R^0 decreased with increasing Al content. The second group of catalysts composed by Al_2O_3 and Al-rich Mg_yAlO_x samples ($r > 0.5$) was highly active for converting 2-propanol via elimination reactions. On these samples, R^0 increased with increasing r (Fig. 7).

Furthermore, it was observed that MgO and Mg-rich Mg_yAlO_x samples ($r \leqslant 0.5$) selectively formed acetone (dehydrogenation product) whereas Al_2O_3 and Al-rich samples ($r > 0.5$) were highly selective to the dehydration product, C_3=. Fig. 8 presents the product distribution for 2-propanol conversion reactions on MgO, Al_2O_3, and Mg_yAlO_x mixed

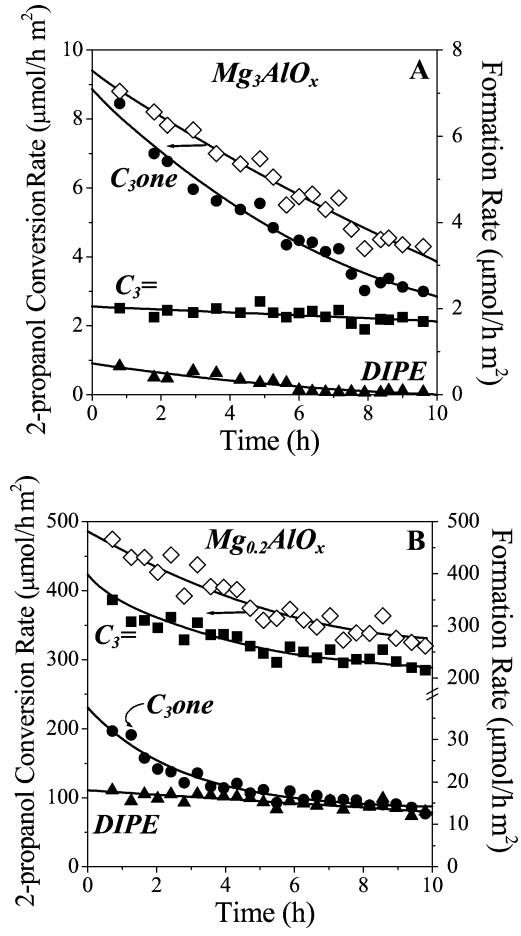

Fig. 6. 2-propanol decomposition reactions over (A) Mg_3AlO_x and (B) $Mg_{0.2}AlO_x$ samples. $T = 533$ K; $P_T = 100$ kPa; N_2/2-propanol = 15 (molar).

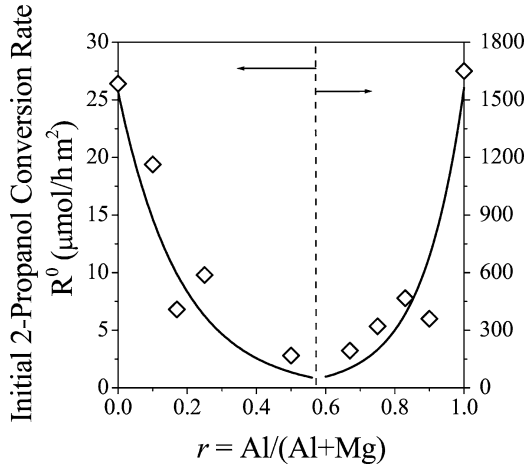

Fig. 7. Initial 2-propanol conversion rate (R^0) over MgO, Al_2O_3, and Mg_yAlO_x catalysts. $T = 533$ K; $P_T = 100$ kPa; N_2/2-propanol = 15 (molar).

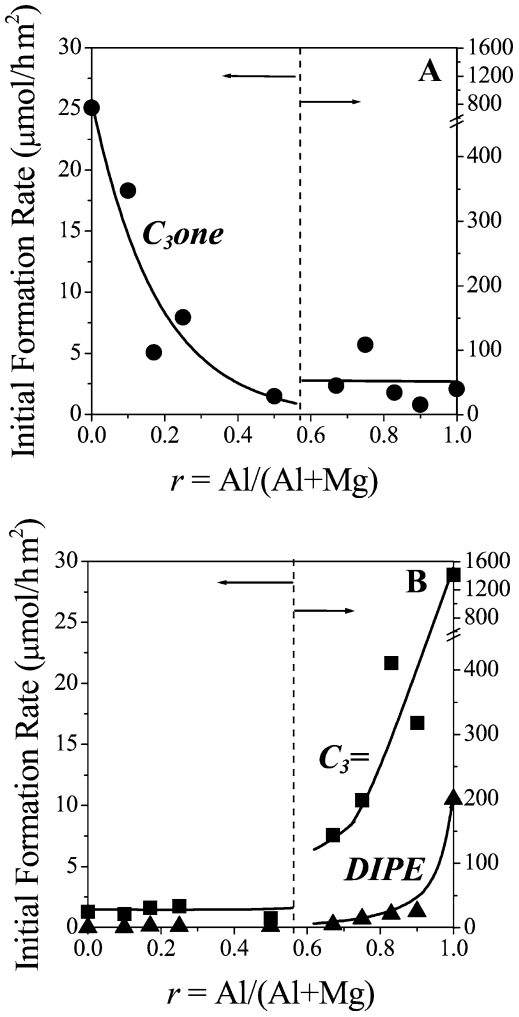

Fig. 8. Product distribution for 2-propanol conversion reactions on MgO, Al_2O_3, and Mg_yAlO_x samples. Initial formation rates as a function of sample composition. (A) Dehydrogenation reaction product, (B) dehydration and coupling-dehydration reaction products. $T = 533$ K; $P_T = 100$ kPa; N_2/2-propanol = 15 (molar).

oxides as a function of the chemical composition. At low Al contents ($r \leqslant 0.5$), acetone formation was favored (Fig. 8A) whereas dehydration products were practically negligible (Fig. 8B). Contrarily, the formation rates of $C_3=$ and DIPE increased with increasing Al content on Mg_yAlO_x samples with $r > 0.5$. The formation rate of $C_3=$ on alumina was three times higher than on $Mg_{0.2}AlO_x$, the most active Mg_yAlO_x oxide sample (Fig. 8B).

Additional catalytic experiments were carried out on Mg_yAlO_x, MgO, and Al_2O_3 samples to determine the activation energy (E_a) and frequency factor (A) for $C_3=$ formation reaction. These parameters were calculated by measuring initial $C_3=$ formation rates ($R^0_{C_3=}$) in the range of 523–553 K at a constant 2-propanol feed concentration and assuming zero-order kinetics [20]. No calculation of the kinetic parameters for the dehydrogenation reaction to acetone was attempted due to the fast deactivation process affecting sites involved in this reaction (Fig. 6).

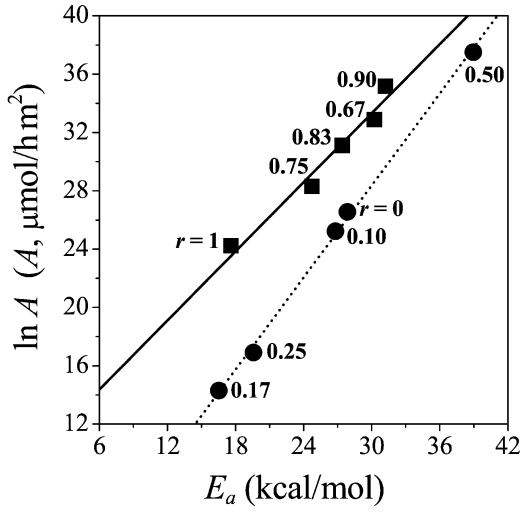

Fig. 9. Compensation effect for dehydration of 2-propanol to propylene on MgO, Al_2O_3, and Mg_yAlO_x samples. $T = 523$–553 K; $P_T = 100$ kPa; N_2/2-propanol = 15 (molar), $r = Al/(Al + Mg)$.

Therefore, according to the Arrhenius law, Eq. (1) was used to calculate parameters E_a and A:

$$\ln R^0_{C_3=} = \ln A - E_a/RT. \quad (1)$$

The calculated E_a and A values for $C_3=$ formation on all the catalysts are represented in Fig. 9. A linear correlation in this semilogarithmic plot known as the "Constable Relation," Eq. (2), is indicative of the existence of a "Compensation Effect" [36]

$$\ln A = mE_a + c. \quad (2)$$

By applying Eq. (2), two compensation lines were obtained on our set of samples, as can be observed in Fig. 9. One compensation line involves Mg-rich catalysts ($r \leqslant 0.5$) and the other, Al-rich samples ($r > 0.5$).

4. Discussion

4.1. Effect of the acid–base properties of Mg_yAlO_x catalysts on the reaction pathways

2-Propanol elimination reactions on Mg–Al mixed oxides, MgO, and Al_2O_3 form dehydrogenation and dehydration products via reaction pathways occurring on dual acid–base pairs that combine acid and base sites of different nature and strength.

In general, dehydration of alcohols may occur through three different mechanisms, E_1, E_2, and E_{1cB} that differ in the configuration of the transition state. Based on the literature [20] and our previous results [17,18], and taking into account the acid–base surface properties of the samples used in this work, 2-propanol dehydration through an E_1 mechanism might be excluded since it requires catalysts containing strong electron pair acceptor sites [37]. Dehydration of

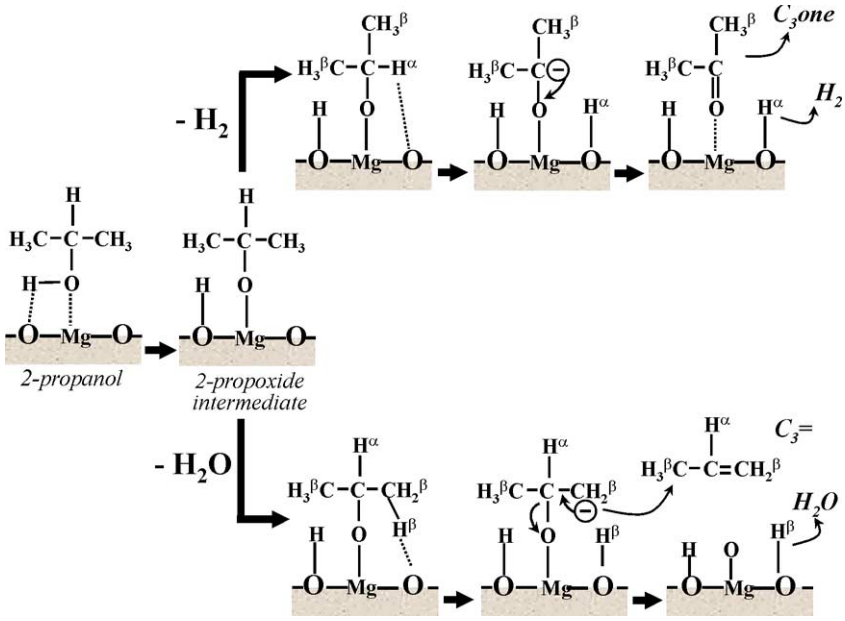

Scheme 2. Formation of C_3one and C_3= via E_{1cB} mechanisms on Mg-rich Mg_yAlO_x catalysts.

2-propanol on Mg_yAlO_x catalysts would take place therefore via E_{1cB} or E_2 mechanisms depending on the catalyst acid–base properties. Furthermore, the E_{1cB} mechanism also accounts for 2-propanol dehydrogenation reaction in a parallel pathway after formation of a common alkoxy intermediate [20] as discussed below.

4.1.1. Reaction pathways on Mg-rich Mg_yAlO_x catalysts

The E_{1cB} dehydration or dehydrogenation mechanism requires acid–base sites of imbalanced strength, i.e., weak Lewis acid and strong Brønsted base sites such as the Mg^{2+}–O^{2-} pairs in pure MgO. In the first step of the E_{1cB} mechanism, 2-propanol is adsorbed through the O–H bond on an acid–base pair site with formation of a surface 2-propoxide intermediate (Scheme 2). The base site attacks the most acidic proton of the 2-propanol molecule (alcoholic hydrogen) whereas the acid site interacts with the oxygen of the alcohol function, thereby activating the rupture of the O–H bond.

The subsequent abstraction of H^{α} or H^{β} from the 2-propoxide intermediate leads to C_3one or C_3=, respectively, via parallel pathways (Scheme 2). In both routes, a carbanion intermediate is formed as a consequence of the proton detachment by the basic catalyst. Predominant formation of either ketone or olefin will depend therefore on the relative acidity of H^{α} and H^{β} and on the catalyst dehydrogenating-dehydrating properties, i.e., on the basic properties of the acid–base pairs.

In a previous work [23], we studied 2-propanol conversion on alkali-promoted MgO and found that these catalysts are typical E_{1cB} materials that form slightly more C_3one than C_3=. We also observed that the C_3= formation rate correlated linearly with the density of strong basic sites (low coordination O^{2-}), whereas that of C_3one depended on the density of medium-strength basic sites (oxygen in Mg^{2+}–O^{2-} pairs). These results showed that C_3= formation from 2-propanol via an E_{1cB}-like mechanism on strongly basic catalysts requires stronger basic sites than 2-propanol dehydrogenation to C_3one.

In contrast to the alkali-promoted MgO catalysts studied before, Mg-rich Mg_yAlO_x samples ($r \leqslant 0.5$) are significantly more active for transforming 2-propanol to acetone than to C_3= (Fig. 8). Mg-rich Mg_yAlO_x mixed oxides are also typical E_{1cB} catalysts since they contain a high relative contribution of Mg^{2+}–O^{2-} pairs (CO_2 TPD, M-peak, Table 2) which are responsible for the dehydrogenating activity. The decrease of the C_3one formation rate as the Al content increases in Mg-rich samples (Fig. 8A) parallels, in fact, the decline of the density of Mg^{2+}–O^{2-} pairs (Table 2). Mg-rich Mg_yAlO_x samples showed a poor activity for converting 2-propanol to C_3= (Fig. 8B), probably because isolated O^{2-} on these samples are not as strong as those present on alkali-promoted MgO to detach a H^{β} through an E_{1cB} dehydration mechanism, as depicted in Scheme 2.

To get more insight on the kinetics of elimination reactions, we measured the kinetic parameters for the conversion of 2-propanol to C_3= and found the existence of a compensation effect for Mg-rich Mg_yAlO_x samples (Fig. 9, dotted line). The compensation effect is generally observed in two cases [36,38,39]: (i) same catalyst with a group of reactants having analogous molecular structures, or (ii) same reactant with a group of catalysts of the same family [40]. Results of Fig. 9 correspond to the latter case and indicate that 2-propanol dehydration to C_3= on Mg-rich Mg_yAlO_x proceeds through the same mechanism and transition state [36]. A compensation behavior for 2-propanol elimination reactions can be also observed in results previously reported on

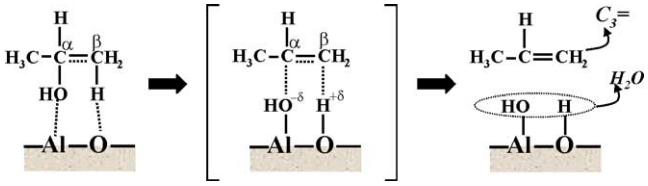

Scheme 3. Formation of $C_3=$ via E_2 mechanism on Al-rich Mg_yAlO_x catalysts.

both base [22,41] and acid [40,42] catalysts and summarized by Galwey [39].

The compensation effect found on Mg-rich samples for $C_3=$ formation may be explained by gradual transformations of surface site energy distribution (strength of the acid–base sites) (Figs. 3–5) and catalyst structure (substitution of Mg^{2+} for Al^{3+} in the MgO lattice) (Figs. 1 and 2), both caused by changes in the catalyst composition, as will be discussed in detail in Section 4.2.

4.1.2. Reaction pathways on Al-rich Mg_yAlO_x catalysts

On Al-rich Mg_yAlO_x samples ($r > 0.5$) the required dehydration steps occurred much faster than on Mg-rich samples and $C_3=$ became the predominant reaction product (Fig. 8B). This result may be explained by considering that the reaction mechanism shifts from E_{1cB} to E_2 when the catalyst acidity increases. In contrast to E_{1cB} dehydration mechanism, the E_2 elimination occurs in a single step without formation of an ionic intermediate (Scheme 3). Dehydration via an E_2 mechanism takes place on acid–base pair sites of similar strength, i.e., a moderately acidic Lewis site and an intermediate-strength Brønsted base site [20], such as the Al^{3+}–O^{2-} pairs of Al_2O_3, which is a typical E_2 catalyst [42]. The observed increase of the dehydration rate with the catalyst Al content on Al-rich samples (Fig. 8B) would reflect then the concomitant increase of the surface Al^{3+}–O^{2-} pair concentration (Table 2).

Bond et al. [36] introduced the concept of multiple lines in Constable plots and showed that a change in the catalyst composition may shift the compensation line to another one that is characteristic of a different transition state. Two compensation lines corresponding to Mg-rich ($r \leqslant 0.5$) and Al-rich samples ($r > 0.5$), respectively, were obtained on our catalysts for 2-propanol dehydration to $C_3=$ (Fig. 9). This result gives additional evidence for the assumption that the dehydration reaction mechanism shifts from E_{1cB} (Mg-rich catalysts) to E_2 (Al-rich catalysts), probably reflecting the fact that on Al-rich Mg_yAlO_x samples the concentration of surface Al^{3+}–O^{2-} dual sites becomes dominant compared to that of Mg^{2+}–O^{2-} pairs. Specifically, the critical chemical composition regarding the change of the reaction mechanism corresponded to a r value of about 0.5 since the $C_3=$ formation rate on Mg_1AlO_x ($r = 0.5$) was two orders of magnitude lower than on $Mg_{0.5}AlO_x$ ($r = 0.67$). However, this abrupt increase of the $R^0_{C_3=}$ value cannot be straightforward related to an increase in the sample surface acidity because the acid site density increased by only a factor of 1.5 from Mg_1AlO_x to $Mg_{0.5}AlO_x$ (Table 2). The increase of the Al content causes significant transformations of the oxide structure and generates different bulk phases that must be taken into account for explaining the catalytic performance of the samples. This effect of the solid structure on catalytic activity will be specifically discussed in the next section.

Alumina and Al-rich Mg_yAlO_x samples ($r > 0.5$) preferentially convert 2-propanol to $C_3=$ but also form C_3one (Fig. 8A). Selectivity to C_3one on these samples was typically lower than 10% and decreased with increasing Al content, but C_3one formation rates were similar or slightly higher than those measured on Mg-rich Mg_yAlO_x samples. However, on Al-rich samples, the concentration of surface Al^{3+}–O^{2-} pairs predominates over that of Mg^{2+}–O^{2-}, and we can exclude therefore that formation of C_3one occurs via a conventional E_{1cB} mechanism like the one depicted in Scheme 2 for Mg-rich samples.

Previous work on decomposition of alcohols on moderately acidic oxides [43–47] report that alcohols undergo mainly dehydration reactions but also produce aldehydes or ketones by dehydrogenation. Several authors proposed that alcohol dehydrogenation occurs via H^α or H^β abstraction as hydride on M^{n+}–O^{2-} pairs (M = metal cation): Nondek and Sedlacek [43] postulated the abstraction of H^α as H^- on Cr_2O_3 while Chung et al. [44] considered the abstraction of H^β followed by hydride transfer on ZnO. Wang et al. [45] suggested that dehydrogenation of 2-propanol on alumina proceeds by abstraction of H^α on the base sites supplied by aluminum defects within the structure. Rekoske et al. [46] studied 2-propanol dehydrogenation on TiO_2 and found that selectivity toward acetone improves by increasing the water concentration in the feed. Then, they postulated that surface OH^- groups take part in the H^α abstraction and that the hydroxyl and alkoxide groups are bound to the same Ti cation. Similarly, Pepe et al. [47] reported a loss of acetone formation activity on α-Al_2O_3 exposed to intense dehydroxylation by outgassing at high temperatures (1123 K). Both groups sustained, on the other hand, that the presence or absence of surface hydroxyls has no influence on the dehydration activity of those materials [46,47].

Thus, there is a general agreement in the literature about that the mechanism for dehydrogenation on moderately acidic catalysts involves a H^α abstraction step, but the nature of the active site that promotes that step is still a matter of controversy. Concerning our Mg_yAlO_x samples synthesized at relatively low temperatures (673 K), results of NH_3 TPD shown in Fig. 5 and Table 2 indicate a relevant contribution of surface hydroxyls (L-peak) to the total density of acid sites. Table 2 also shows that the density of Brønsted OH sites increases with increasing the Al content, thereby suggesting a higher hydroxylation of the Al-rich Mg_yAlO_x catalysts. These observations are in agreement with previous results obtained by XPS (X-ray photoelectron spectroscopy) showing that on Mg_yAlO_x oxides the O 1s binding energy increases gradually from the value typical of surface O^{2-}

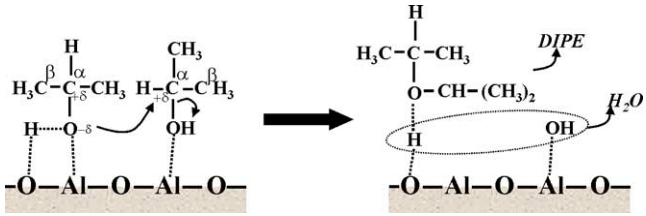

Scheme 4. Formation of DIPE on Al-rich Mg_yAlO_x catalysts.

on Mg-rich samples to that characteristic of surface OH^- on Al-rich catalysts [17].

Therefore, we postulate that C_3one formation on Al-rich Mg_yAlO_x catalysts would proceed by alkoxide formation and subsequent H^α abstraction via an E_{1cB}-like mechanism, probably involving OH^- groups vicinal to Al^{3+} cations.

Formation of DIPE, another 2-propanol dehydration product obtained in minor amounts on Al-rich Mg_yAlO_x samples, may also be interpreted in terms of an E_2 mechanism [20] (Scheme 4). Contrarily to our previous results obtained for primary alcohol conversion on similar Mg–Al mixed oxides [17,18], we found here that DIPE formation rates are lower than 2-propanol conversion rates to $C_3=$ (Fig. 8B). Jain and Pillai [48] demonstrated that dehydration of 2-propanol on alumina proceeds at a higher rate toward $C_3=$ than toward the competitive DIPE formation, even when the former reaction has a higher activation energy. This result may be explained by considering that despite that secondary alcohols are more easily dehydrated than primary alcohols [40], ether formation from 2-propanol is not favored because it is a second-order reaction that involves the adsorption of two branched alcohol molecules on neighboring active sites offering different acid–base properties [17,48,49]. Scheme 4 shows the adsorption of one alcohol molecule on an acid–base pair and the other on a Lewis acid site. In addition, DIPE has four branched methyl groups and therefore its bulky structure impedes the free motion of the molecule within the catalyst pores.

However, in contrast to the ether formation mechanism shown in Scheme 4, several authors [50,51] have proposed that formation of ethers by an E_2 mechanism may involve weak Brønsted acid sites as those provided by the OH^- groups in Al-rich Mg_yAlO_x samples rather than Lewis acid sites such as Al^{3+} cations. From the present results, participation of the Brønsted acid sites cannot be ruled out since DIPE formation (Fig. 8B) is favored on the most hydroxylated samples (NH_3 TPD, L-peak, Table 2).

4.2. Structural effects and catalytic performance

The abrupt increase of 2-propanol conversion rate observed when the sample Al content reaches an r value slightly higher than 0.5 (Fig. 7) cannot be explained only in terms of density of surface active sites. Also, the formation rates of C_3one, $C_3=$, or DIPE showed no direct correlation with the acid or base site densities determined by NH_3 or CO_2 TPD, respectively. The catalytic performance of Mg_yAlO_x catalysts seems to be related not only to the surface density of active sites but also to the nature of the bulk structure and transformations in the cation (Mg^{2+} or Al^{3+}) environment induced by changing the chemical composition. For instance, MgO was the most active catalyst for 2-propanol elimination reactions among the Mg-rich Mg_yAlO_x samples ($r \leqslant 0.5$), but incorporation of just 5.8 wt% Al (sample Mg_9AlO_x) decreased the catalytic activity by a 25% (Fig. 7). Similarly, sample $Mg_{0.11}AlO_x$ contains only 3.4 wt% Mg but was 80% less active than pure Al_2O_3, the most active sample of the Al-rich catalysts ($r > 0.5$).

4.2.1. Structural effects in Mg-rich Mg_yAlO_x catalysts

The lattice parameter a of hydrotalcite precursors containing low Al amounts ($r \leqslant 0.5$) decreased monotonically with increasing r (Table 1). This contraction of the hydrotalcite unit cell appears to be caused by formation of a solid solution, which is structurally stable because Al^{3+} cations replace larger Mg^{2+} cations within the brucite structure. Thus, Al^{3+} can randomly and uniformly replace Mg^{2+} in octahedral sites within brucite layers without disrupting the layer structure.

During thermal decomposition of Mg-rich hydrotalcite precursors ($r \leqslant 0.5$), formation of MgO (Mg^{2+} cations in octahedral sites) takes place. The fact that no segregated aluminum phase was detected, indicates that either the Al^{3+} cations totally incorporate into the salt-rock structure of the periclase phase or they form an amorphous AlO_x or Mg–Al oxide phase not detectable by XRD.

Several authors have shown by ^{27}Al NMR that Al^{3+} cations in calcined hydrotalcites are coordinated to oxygen in octahedral (Al_{Oh}) and tetrahedral (Al_{Td}) environments, with a clear predominance of aluminum in octahedral positions [13,24,25,29,52,53]. In agreement with those previous reports, our ^{27}Al NMR results of Figs. 1 and 2 indicate that Mg-rich oxides contain both Al_{Td} and Al_{Oh}. Then, Al^{3+} coordination changes only partially from octahedral in the parent precipitated precursor to tetrahedral in the resulting mixed oxide.

The break of the fitting line for Al_{Oh} in Fig. 1 suggests that Al^{3+} cations in octahedral coordination take part of different bulk structures in Mg-rich ($r \leqslant 0.5$) and Al-rich ($r > 0.5$) samples, respectively. In Mg-rich oxides, only MgO was detected; Al_{Oh} may be located in the MgO framework forming small Al_{Oh}–O–Mg domains not detectable by XRD. The diminution of the Al_{Oh}/Al_{Td} ratio at increasing Al contents (Fig. 2) is probably due to the fact that the Al^{3+} cations progressively leave octahedral sites to form incipient domains of partially inverse spinel-related ordering in which part of the Al^{3+} cations are tetrahedrally coordinated in Al_{Td}–O–Mg species as suggested by Shen et al. [24].

The capacity of these Mg-rich oxides to easily regenerate the parent hydrotalcite when exposed to ambient moisture

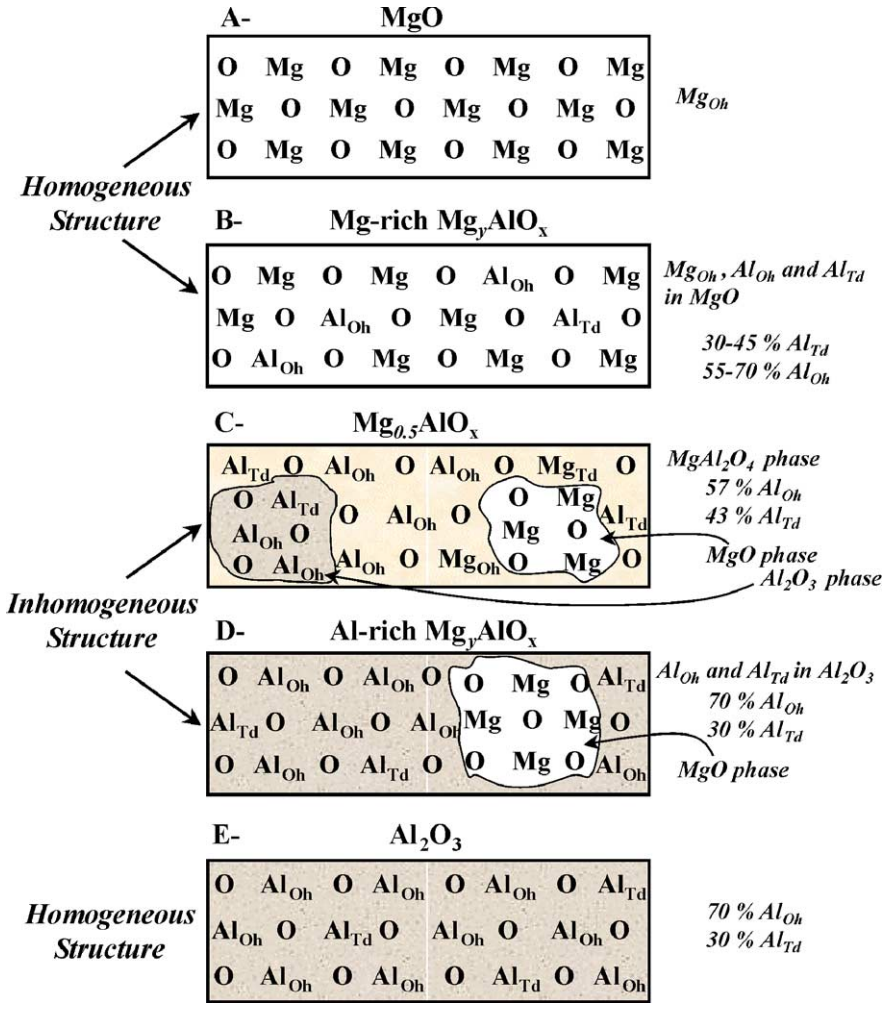

Scheme 5. Structural changes produced by increasing the Al content in Mg_yAlO_x catalysts.

excludes segregation of bulk alumina or spinel phases and supports the fact that both Al_{Oh} and Al_{Td} cations remain closely associated to the MgO matrix [29,53]. In fact, we have detected on Mg-rich Mg_yAlO_x oxides stored in lab vials and not submitted to heat treatment before NMR analysis only one resonance peak with a chemical shift at around 9 ppm, which is typical of Al_{Oh} in hydrotalcite structures [29,53].

A simplified scheme of the structural changes occurring in Mg_yAlO_x samples when the Al content increases is shown in Scheme 5. The structure of MgO and Mg-rich mixed oxides are depicted in Scheme 5A and 5B, respectively. In the homogeneous structure of Mg-rich samples, Al^{3+} cations are incorporated into the MgO matrix, forming small Mg–Al domains which at higher Al contents give rise to formation of separate Al-rich and $MgAl_2O_4$ bulk phases as shown in Scheme 5C for sample $Mg_{0.5}AlO_x$ (Table 1).

The intimate contact between Mg^{2+} and Al^{3+} cations in the MgO framework may explain the catalytic performance of Mg-rich Mg_yAlO_x catalysts. In fact, the presence of more electronegative Al^{3+} cations in the environment of the Mg^{2+}–O^{2-} pairs decreases the average basicity of MgO with the consequent drop of the acetone formation rate (Fig. 8A). The activity for 2-propanol dehydrogenation decreases further with increasing Al content because the environment of the Mg^{2+}–O^{2-} pairs into the MgO matrix contains a higher concentration of Al^{3+} cations. However, since on Mg-rich Mg_yAlO_x catalysts phase segregation does not occur, 2-propanol dehydrogenation mechanism is not changed by varying the r ratio.

The structural characteristics of Mg-rich Mg_yAlO_x catalysts also account for the low dehydrating properties of these samples (Fig. 8B). The substitution of Mg^{2+} for Al_{Oh} in the MgO framework produces a cationic vacancy that may behave as an acid site; however, since it will be surrounded by coordinatively unsaturated oxygen anions, the solid solution will display low acidic properties. The acid site density measured by NH_3 TPD was almost constant on these samples (Table 2), thereby confirming that Al^{3+} cations are in the oxidic environment of the MgO matrix where dehydration reactions are not favored. This is in agreement with the findings of McKenzie et al. [25] who showed that Al^{3+} cations associated to MgO are less active to dehydrate 2-propanol than those of alumina.

4.2.2. Structural effects in Al-rich Mg_yAlO_x catalysts

The rate of 2-propanol dehydration to $C_3=$ on $Mg_{0.5}AlO_x$ ($r = 0.67$) is about two orders of magnitude higher than on Mg_1AlO_x ($r = 0.5$) (Fig. 8B). We explained this result in terms of a shift in the reaction mechanism from E_{1cB} to E_2 caused not only by a change of the nature and density of the surface acid sites but also of the structure of the mixed oxides.

XRD analysis showed that, in contrast to Mg-rich precursors ($r \leqslant 0.5$), Al-rich precursors ($r > 0.5$) were not able to accommodate additional Al^{3+} cations in the brucite layers of the hydrotalcite structure as indicated by both the invariance of the hydrotalcite lattice parameter a and the formation of additional gibbsite and brucite phases on these samples (Table 1). Furthermore, in precursors with $r \geqslant 0.83$ Mg^{2+} and Al^{3+} cations appeared only in separate hydroxide phases (brucite and gibbsite) losing the structural linkage they had in the hydrotalcite structure but maintaining the octahedral coordination.

Then, low-temperature thermal decomposition of structurally heterogeneous Al-rich hydrated precursors ($r > 0.5$) led to the formation of heterogeneous mixed oxides, all of them containing a separate quasi-amorphous Al_2O_3 phase. In sample $Mg_{0.5}AlO_x$ ($r = 0.67$), besides MgO and Al_2O_3, bigger Mg–Al domains than those present in Mg-rich Mg_yAlO_x catalysts form a bulk $MgAl_2O_4$ spinel with 43% Al_{Td} as depicted in Scheme 5C. Formation of this new species suggests that both Al_{Oh} and Al_{Td} cations in part have left the MgO lattice as the Al content increased and therefore, Al^{3+} and Mg^{2+} cations lost their intimate contact. The Al_{Oh}/Al_{Td} ratio increased with r (Fig. 2) reflecting a concomitant increase of alumina phase concentration. Mg_yAlO_x catalysts with $r \geqslant 0.83$ did not contain Mg–Al spinel-like phase (Scheme 5D) and structurally resemble low-crystallinity alumina and magnesia, as indicated by the Al_{Oh}/Al_{Td} ratio of about 2.3 measured on these samples (Fig. 2). The catalyst surface might be envisaged as pure alumina covered by MgO patches whose sizes become smaller as the Al content increases.

Formation of separate Al and Mg phases in Al-rich mixed oxides was consistent with results obtained by NMR. In fact, these samples exposed to ambient moisture showed Al_{Td} and Al_{Oh} resonance peaks at chemical shifts similar to those of the corresponding freshly calcined samples, thereby indicating that no reconstruction of binary Mg–Al hydrotalcite precursors took place.

In summary, Al-rich Mg_yAlO_x catalysts ($r > 0.5$) are structurally heterogeneous mixed oxides that contain a separate quasi-amorphous Al_2O_3-like phase. Segregation of the alumina phase occurs for sample $Mg_{0.5}AlO_x$ ($r = 0.67$) and provides dual Al^{3+}–O^{2-} active sites that dehydrate 2-propanol to $C_3=$ at high turnover rates via an E_2 mechanism and also form DIPE. Increasing the Al content further increases the surface concentration of Al_2O_3-like phase, thereby favoring 2-propanol dehydration reactions.

5. Conclusions

2-Propanol elimination reactions on Mg_yAlO_x mixed oxides yield dehydrogenation and dehydration products via reaction pathways occurring on dual acid–base sites. The chemical nature and acid–base properties of these active sites (Mg^{2+}–O^{2-} or Al^{3+}–O^{2-}) as well as the sample bulk structure depend on chemical composition.

In Mg-rich oxides Al^{3+} replace Mg^{2+} into MgO matrix forming homogeneous solids that contain mainly surface Mg^{2+}–O^{2-} active sites. Dehydration and dehydrogenation reactions proceed through E_{1cB}-like mechanisms sharing a common 2-propoxide intermediate, but 2-propanol is preferentially transformed to acetone because Mg^{2+}–O^{2-} sites efficiently catalyze dehydrogenation steps by promoting the α-hydrogen abstraction from the alkoxide group. Increasing the concentration of more electronegative Al^{3+} cations in the environment of the Mg^{2+}–O^{2-} pairs decreases the average basicity of MgO with the consequent drop of the acetone formation rate.

Al-rich Mg_yAlO_x samples convert 2-propanol mainly to propylene via an E_2 mechanism occurring on dual Al^{3+}–O^{2-} sites. The shift in the dehydration reaction mechanism from E_{1cB} (Mg-rich catalysts) to E_2 (Al-rich catalysts) is produced by a change of the active site from Mg^{2+}–O^{2-} to Al^{3+}–O^{2-} and by significant modifications of the oxide structure both caused by the increase of the aluminum content in the samples. Al-rich Mg_yAlO_x samples are heterogeneous mixed oxides that contain a separate quasi-amorphous Al_2O_3-like phase. Nucleation of a separate stable Al-rich phase provides dual Al^{3+}–O^{2-} active sites that dehydrate 2-propanol to propylene at high turnover rates. The observed increase of the dehydration rate with the catalyst Al content reflects then a concomitant increase of the surface Al^{3+}–O^{2-} pair concentration.

The catalytic and structural transition from homogeneous Mg-rich to heterogeneous Al-rich mixed oxides occurs for samples containing Mg/Al ratios between 0.5 and 1, and seems to be essentially related to a change in the homogeneity and phase composition of parent coprecipitated precursors. Mg-rich hydrotalcite-like precursors contain Al^{3+} and Mg^{2+} cations randomly distributed in the octahedral sites within brucite layers. Decomposition of these hydrotalcite precursors at 673 K yields homogeneous Mg_yAlO_x mixed oxides that contain the Al^{3+} cations totally incorporated into the MgO framework. In Al-rich coprecipitated precursors, Mg^{2+} and Al^{3+} cations appear in separate brucite and gibbsite hydroxide phases, thereby losing the structural linkage they had in the hydrotalcite structure. Thermal decomposition of heterogeneous Al-rich hydrated precursors forms heterogeneous Mg_yAlO_x mixed oxides, all of them containing separate low-crystallinity magnesia and alumina phases.

Acknowledgments

The authors thank the Universidad Nacional del Litoral, Santa Fe (CAID 2000 17-1-47) and CONICET (Argentina) for the financial support of this work. They also thank Dr. A. Corma and Dr. T. Blasco Lanzuela for the use of the NMR facilities at the Instituto de Tecnología Química, Valencia, Spain. V.K.D. thanks the Agencia Española de Cooperación Internacional (Spain) and Estrella Mateos for technical assistance.

References

[1] F. Cavani, F. Trifiro, A. Vaccari, Catal. Today 11 (1991) 173.
[2] V.L. Constantino, T.J. Pinnavaia, Inorg. Chem. 34 (1995) 883.
[3] F. Prinetto, G. Ghiotti, R. Durand, D. Tichit, J. Phys. Chem. B 104 (2000) 11117.
[4] A. Vaccari, Catal. Today 41 (1998) 53.
[5] K.K. Rao, M. Gravelle, J. Sanchez Valente, F. Figueras, J. Catal. 173 (1998) 115.
[6] J.I. Di Cosimo, V.K. Díez, C.R. Apesteguía, Appl. Clay Sci. 13 (1998) 433.
[7] J.C.A.A. Roelofs, A.J. Van Dillen, K.P. de Jong, Catal. Today 60 (2000) 297.
[8] A.H. Padmasri, V.D. Kumari, P.K. Rao, in: T.S.R. Prasada Rao, G. Murali Dhar (Eds.), Studies in Surface Science and Catalysis, Vol. 113, Elsevier, Amsterdam, 1998, p. 563.
[9] S. Velu, C.S. Swamy, Catal. Lett. 40 (1996) 265.
[10] A. Corma, S. Iborra, J. Primo, F. Rey, Appl. Catal. 114 (1994) 215.
[11] B.M. Choudary, M.L. Kantam, C.R.V. Reddy, K.K. Rao, F. Figueras, J. Mol. Catal. A Chem. 146 (1999) 279.
[12] P. Kumbhar, J. Sanchez-Valente, F. Figueras, J. Chem. Soc., Chem. Commun. (1998) 1091.
[13] H. Schaper, J.J. Berg-Slot, W.H.J. Stork, Appl. Catal. 54 (1989) 79.
[14] W. Kagunya, Z. Hassan, W. Jones, Inorg. Chem. 35 (1996) 5970.
[15] F. Malherbe, J.P. Besse, S.R. Wade, W.J. Smith, Catal. Lett. 67 (2000) 197.
[16] J.J. Alcaraz, B.J. Arena, R.D. Gillespie, J.S. Holmgren, Catal. Today 43 (1998) 89.
[17] J.I. Di Cosimo, V.K. Díez, M. Xu, E. Iglesia, C.R. Apesteguía, J. Catal. 178 (1998) 499.
[18] J.I. Di Cosimo, C.R. Apesteguía, M.J.L. Ginés, E. Iglesia, J. Catal. 190 (2000) 261.
[19] J.I. Di Cosimo, G. Torres, C.R. Apesteguía, J. Catal. 108 (2002) 114.
[20] A. Gervasini, J. Fenyvesi, A. Auroux, Catal. Lett. 43 (1997) 219.
[21] S.V. Bordawekar, E.J. Doskocil, R. Davis, Catal. Lett. 44 (1997) 193.
[22] Z.G. Szabó, B. Jóvér, R. Ochmacht, J. Catal. 39 (1975) 225.
[23] V.K. Díez, J.I. Di Cosimo, C.R. Apesteguía, Catal. Today 63 (2001) 53.
[24] J. Shen, M. Tu, C. Hu, J. Solid State Chem. 137 (1998) 295.
[25] A.L. McKenzie, C.T. Fishel, R.J. Davis, J. Catal. 138 (1992) 547.
[26] K. Sohlberg, S.J. Pennycook, S.T. Pantelides, Chem. Eng. Commun. 181 (2000) 107.
[27] J.D. Dunitz, L.E. Orgel, J. Phys. Chem. Solids 3 (1957) 318.
[28] A. Navrotsky, O.J. Kleppa, J. Inorg. Nucl. Chem. 29 (1967) 2701.
[29] E.G. Derouane, V. Jullien-Lardo, R.J. Davis, N. Blom, P.E. Hojlund-Nielsen, in: L. Guczi, L. Solymosi, P. Tetenyi (Eds.), New Frontiers in Catalysis, Vol. B, Elsevier, Amsterdam, 1993, p. 1033.
[30] R. Philipp, K. Fujimoto, J. Phys. Chem. 96 (1992) 9035.
[31] T. Kanno, M. Kobayashi, in: M. Misono, Y. Ono (Eds.), Acid–Base Catalysts II, Kodansha–Elsevier, Tokyo, 1994, p. 207.
[32] P. Berteau, B. Delmon, J.L. Dallons, A. Van Gysel, Appl. Catal. 70 (1991) 307.
[33] E. Garrone, F. Stone, in: M. Che, G.C. Bond (Eds.), Adsorption and Catalysis on Oxide Surfaces, Elsevier, Amsterdam, 1985, p. 97.
[34] H. Knozinger, R. Khone, J. Catal. 5 (1966) 264.
[35] P.L. Yue, O. Olaofe, Chem. Eng. Res. Des. 62 (1984) 81.
[36] G.C. Bond, M.A. Keane, H. Kral, J.A. Lercher, Catal. Rev.-Sci. Eng. 42 (3) (2000) 323.
[37] H. Noller, W. Kladnig, Catal. Rev. Sci. Eng. 13 (2) (1976) 149.
[38] M. Boudart, Chem. Eng. Prog. 57 (1961) 33.
[39] A.K. Galwey, Adv. Catal. 26 (1977) 247.
[40] P.L. Yue, O. Olaofe, Chem. Eng. Res. Des. 62 (1984) 167.
[41] E.F. McCaffrey, T.A. Micka, R.A. Ross, J. Phys. Chem. 76 (1972) 3372.
[42] H. Knozinger, H. Buhl, K. Kochloefl, J. Catal. 24 (1972) 57.
[43] L. Nondek, J. Sedlacek, J. Catal. 40 (1975) 34.
[44] M.J. Chung, S.H. Han, K.Y. Park, S.K. Ihm, J. Mol. Catal. 79 (1993) 335.
[45] J.A. Wang, X. Bokini, O. Novaro, T. López, F. Tzompantzi, R. Gómez, J. Navarrete, M.E. Lanos, E. López-Salinas, J. Mol. Catal. 137 (1999) 239.
[46] J.E. Rekoske, M.A. Barteau, J. Catal. 165 (1997) 57.
[47] F. Pepe, F.S. Stone, in: Proceedings of the 5th International Congress on Catalysis, Miami Beach, 1972, pp. 2–137.
[48] J.R. Jain, C.N. Pillai, J. Catal. 9 (1967) 322.
[49] J.C. Balaceanu, J.C. Jungers, Bull. Soc. Chim. Belg. 60 (1951) 476.
[50] H. Noller, G. Ritter, J. Chem. Soc. Faraday Trans. 1 (80) (1984) 275.
[51] P. Canesson, M. Blanchard, J. Catal. 42 (1979) 205.
[52] W.T. Reichle, S.Y. Kang, D.S. Everahardt, J. Catal. 101 (1986) 352.
[53] A. Corma, V. Fornés, F. Rey, J. Catal. 148 (1994) 205.